View metadata, citation and similar papers at core.ac.uk
brought to you by CORE
provided by Open Research Exeter

A machine learning approach for the detection of supporting rock bolts from laser scan data in an underground mine

Jane Gallwey [a, *], Matthew Eyre [a], John Coggan [a]

[a] *Camborne School of Mines, University of Exeter, Penryn, United Kingdom*

* *Corresponding author: Jane Gallwey: j.gallwey@exeter.ac.uk, Tremough Campus, Penryn, United Kingdom, TR109AH*

Keywords: mining; rock bolting; machine learning; laser scanning; object detection

Abstract

Rock bolts are a crucial part of underground infrastructure support; however, current methods to locate and record their positions are manual, time consuming and generally incomplete. This paper describes an effective method to automatically locate supporting rock bolts from a 3D laser scanned point cloud. The proposed method utilises a machine learning classifier combined with point descriptors based on neighbourhood properties to classify all data points as either 'bolt' or 'not-bolt' before using the Density Based Spatial Clustering of Applications with Noise (DBSCAN) algorithm to divide the results into candidate bolt objects. The centroids of these objects are then computed and output as simple georeferenced 3D coordinates to be used by surveyors, mine managers and automated machines. Two classifiers were tested, a random forest and a shallow neural network, with the neural network providing the more accurate results. Alongside the different classifiers, different input feature types were also examined, including the eigenvalue based geometric features popular in the remote sensing community and the point histogram based features more common in the mobile robotics community. It was found that a combination of both feature sets provided the strongest results. The obtained precision and recall scores were 0.59 and 0.70 for the individual laser points and 0.93 and 0.86 for the bolt objects. This demonstrates that the model is robust to noise and misclassifications, as the bolt is still detected even if edge points are misclassified, provided that there are enough correct points to form a cluster. In some cases, the model can detect bolts which are not visible to the human interpreter.

1 Introduction

Rock reinforcement is a crucial element of underground construction. When operating with any underground excavation, an understanding of the rock mass characteristics as an engineering material is critical in ensuring that risks from tunnel collapse are mitigated through the use of ground control methods. Installation of rock bolts is the most widely used form of ground support (Li, 2017). The design of such a system is site dependent and based on the mechanical behaviour of the rock mass, the in-situ stress field and induced stress from the excavation (Hoek and Brown, 1982). In low stress conditions, compression of the ground is needed to ensure loose blocks do not fall. This can be achieved either by using spot bolting of discrete blocks or by a systematic bolting pattern. Spot bolting is carried out where needed without following a set spacing, whereas systematic patterns are used to add a compression arch to the rock mass, reducing the potential for unravelling. Schach et al (1979) shows that an increase in bolt spacing leads to less interaction of neighbouring bolts, reducing the size of the compression zone to a point at which the bolts no longer provide a wide coverage leading to potential fall of ground. To ensure the required level of compressive cover is produced, it is important that correct installation of bolt patterns is carried out. Reconciliation of installed bolts is therefore an important part of the ground management process to ensure safe working underground.

Current methods of documenting rock bolt installation are usually hand sketch based and not comprehensive (Öberg, 2013) due to the large volume of bolts that have to be recorded and the difficulty and time-consuming nature of manually surveying such data, along with the associated human error for this type of repetitive task. Another difficulty is that in many applications the entire surface is covered with shotcrete after installation, rendering the exact locations of the rock bolts unknown or challenging to discern (Öberg, 2013). Automatically detecting and recording the 3D coordinates of rock bolts either retrospectively or at installation would allow for greater quality assurance and quality control, providing a detailed record of exactly where rock bolts have been installed. These records also would be critical in a fall of ground situation, where the exact bolting configuration that was installed prior to the incident must be determined. Advancements in remote sensing techniques and machine learning algorithms could allow this bolting pattern information to be obtained. However, currently the mining sector is not fully utilising these new technologies despite being well placed to employ them due to a widespread adoption of laser scanners and other high resolution surveying technologies both onboard vehicles and as standalone survey technologies (Body, 2014).

To date, image based photogrammetric systems for automatically inspecting civil engineering tunnels have been the primary research focus in this area. A review of these techniques is given in Attard et al., (2018) and successful implementations for crack detection by Huang et al. (2018) and moisture mark detection by Zhao et al. (2020), demonstrating the power of remote sensing and machine learning for underground infrastructure management. However, passive remote sensing methods such as photogrammetry can be problematic underground, particularly in mines, due to challenges from uneven illumination and dust (Gikas, 2012). Active systems such as laser scanning circumvent these issues, by measuring using multiple high speed laser pulses emitted from the instrument itself (Eyre et al., 2016). The data obtained from a laser scanner is in the form of a 3D point cloud which records the X, Y, Z coordinates of the reflected point in 3D. Most scanners also record the intensity of the laser return and some also use cameras to store an RGB colour value for each point. The primary issue with laser scanners compared to cameras is the size of the data collected and the subsequent difficulty in efficiently processing it. The raw output from the laser scanner is a large unordered set of 3D coordinates with no semantic knowledge of the object they are surveying. This 3D point cloud data is currently used by mines directly for surveying tasks such as change detection, geometric analysis and as-built to design comparison (van der Merwe and Andersen, 2013). In order for this data to be utilised in a wider range of applications such as automated machines, mine information databases and infrastructure monitoring a level of semantic information needs to be added to the data, along with a reduction in the dataset size.

The only directly applicable prior work on this topic is by Martínez-Sánchez et al. (2016). In this paper they built and trained an autoencoder based model to detect not only the rock bolts from laser scan data, but also their orientations and the shotcrete thickness. Their work achieved a very high accuracy of 91% showing that geometric neighbourhood based machine learning algorithms have great potential to solve this engineering and monitoring problem. Laser scanners also have been used in tunnel inspection (Tan et al., 2016, Xu et al., 2018) however, these studies have used the laser scan data to generate intensity images rather than detecting objects from the 3D point cloud data. Soilán et al., (2019) give a full review of the use of laser scanners for infrastructure monitoring; whilst there is minimal published work on detecting discrete objects in an underground environment from laser scanned data, automatically generating an understanding of a scene from point cloud data has been the topic of much research in recent years. Most application oriented work in this field focuses on either identifying roadside objects and road characteristics from surface mobile laser scan data (Yang et al., 2013, Lehtomäki et al., 2016, Soilán et al., 2017 and Balado et al., 2018) or on ground cover classification from aerial LiDAR data (Blomley et al., 2016), (Niemeyer et al., 2014) and (Rau et al., 2015). Properties of these types of surface scenes, such as proliferation of regular vertical objects in streetscapes and a mostly fixed view angle in aerial LiDAR can be leveraged to aid in detecting these types of objects, unlike in the underground environment. Underground terrestrial and mobile laser scan data is complex as it is true 3D data, with the possibility of multiple points sharing the same XY location but possessing different Z values. Approaches used for identification of discrete objects on roads, such as Weinmann et al. (2017) for trees and Lehtomäki et al. (2010) for poles can be considered the closest neighbours, and techniques from these studies can be adapted to the problem of identifying underground features or objects with regard to the particular properties of the underground environment.

The classical method for point cloud object detection is described in Weinmann et al. (2015a) and involves three steps: neighbourhood selection, feature extraction and classification. Other methods that do not follow this framework include directly classifying using Markov networks (Anguelov et al., 2005), (Agrawal et al., 2009) and (Triebel et al., 2006), spectral hashing (Behley et al., 2010) and most recently, approaches using deep learning. Whilst deep learning approaches have shown impressive results (Maturana and Scherer, 2015, Qi et al., 2016, Riegler et al., 2017), the additional model complexity, computational power, training time and the size of the training data required for successful deployment make these methods less attractive for an efficient vehicle-based solution. For this application the classical approach similar to Weinmann et al. (2017) was selected, allowing a low computational burden which is more appropriate for time critical applications such as those deployed on underground vehicles and equipment.

This paper will describe an automated approach for rock bolt identification from laser scan data using machine learning. The method is based on the classical point cloud semantic segmentation technique defined in Weinmann et al., (2015a), but implemented using a more extensive set of features from both the robotics and remote sensing communities, alongside adaptions for the geometry of underground environments. The machine learning element of the research compares the two popular classifiers, a random forest and an artificial neural network. Following the classification, the bolt objects are extracted via clustering and centroid generation. Section 1 outlines the task and examines related work, Section 2 describes the datasets used for model development, Section 3 details the methodology, Section 4 presents the results, Section 5 discusses the finding and Section 6 concludes the work.

2 Datasets

A large amount of labelled data is required to train a machine learning classifier to detect objects. As there are no available datasets of labelled laser scanned rock bolts, a dataset was collected and annotated specifically for this study. The data was collected from a 250m section of underground workings in a small tin and copper mine. This is a good training area, as the slaty nature of the country rock manifests itself as a fair to poor quality rock mass, resulting in extensive spot bolting based on observations of potential block fallouts. The area of interest was surveyed using a terrestrial laser scanning workflow. The scanner was mounted on a static tripod to perform a scan, next the scanner was moved to a position approximately 12m further down the tunnel and another scan was taken. This process was repeated for 25 scans. The individual scans were registered together to make a unified dataset in the point cloud processing software Leica Cyclone. The hardware used was a Leica C10 laser scanner, as used in other underground studies such as Ganić et al. (2011), Chen et al. (2018) and Long et al. (2018). This instrument has a specified accuracy of ± 6mm per point (Long et al., 2018) and the scan resolution at the chosen setting provides a point spacing of 5mm at 5m from the scanner. The scanner was set to record only laser intensities not optical imagery values. This is due to the poor illumination in the mine and the additional time required to take photographs with the inbuilt camera. The final dataset is representative of real world underground scan data, containing laser noise, occlusions and many objects that are neither tunnel nor bolt and it has not been manually cleaned and simplified for improved machine learning results. A sample of the data is shown in Figure 1.

Figure 1: A view of the underground data. Many challeging objects are present including pipes, brackets, ventilation bagging and electrical boxes.The colour scheme is taken from the strength of the laser return.

To generate the training data, the rock bolt points were manually separated from all other points and given the class label 1 'bolt'. All other objects were labelled 0 'not-bolt', including confusion objects such as pipes, brackets and ventilation bagging, alongside the hanging wall, side wall and foot wall surfaces. This dataset was then split into sections for training, cross-validation and testing, as shown in Figure 2. The grey areas are unused and have been reserved for future algorithm testing.

Figure 2: Tunnel showing the areas for training (blue), cross-validation (green) and testing (red).

2.1 Pre-processing

Before the point cloud dataset features can be generated a number of preprocessing steps are carried out, using the open source software CloudCompare (Girardeau-Montaut, 2016). Firstly, the point clouds are shifted from their real-world coordinates to a position near the origin to avoid potential precision loss from processing very large numbers. Next, denoising is carried out using an algorithm which works similarly to a low pass filter. This removes points which are further than a set factor of their neighbours reprojection error onto a plane, where the plane itself is fitted to all points within a specified radius (Girardeau-Montaut, 2016). The denoising settings used a radius of 10cm and a relative error factor of

1. The final step in the base dataset creation is density reduction. Point clouds acquired from laser scanners have a large variation in density due to many factors including an object's distance from the scanner, the scan angle, overlap between neighbouring scans and occlusions. Whilst it is difficult to create new points in areas of low density, it is straightforward to remove points in areas of high density using resampling techniques. For this application the point cloud was spatially resampled to a density of 1 point per cm maximum. Figure 3 shows the distribution of point densities before and after resampling. The resampling algorithm also reduced the total number of points by ~40%. As shown in Figure 3, the density range is now closer to a normal distribution, but still not constant across the point cloud. This is because a constant density is undesirable for real world data, as there will always be areas of low sampling due to occlusions, however, if the majority of the cloud is downsampled to match the lowest density much of the useful detail can be lost. Following density reduction, the dataset contains 10 million labelled laser scanned points.

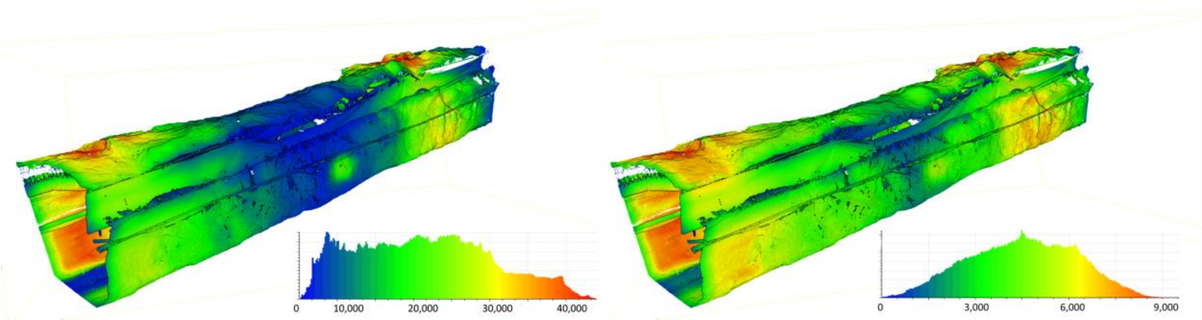

Figure 3: A section of the training data showing the density before (left) and after (right) spatial resampling. The density is measured as the number of points per square meter of tunnel surface. The graphs below each image show the range of data densities, before resampling it ranges from 0-40,000 and after it ranges from 0-9,000.

3 Methodology

The workflow for detecting bolts from the laser scanned point cloud dataset has three primary components: feature descriptor creation, machine learning classification and object creation. An overview of the processing workflow is shown in Figure 4.

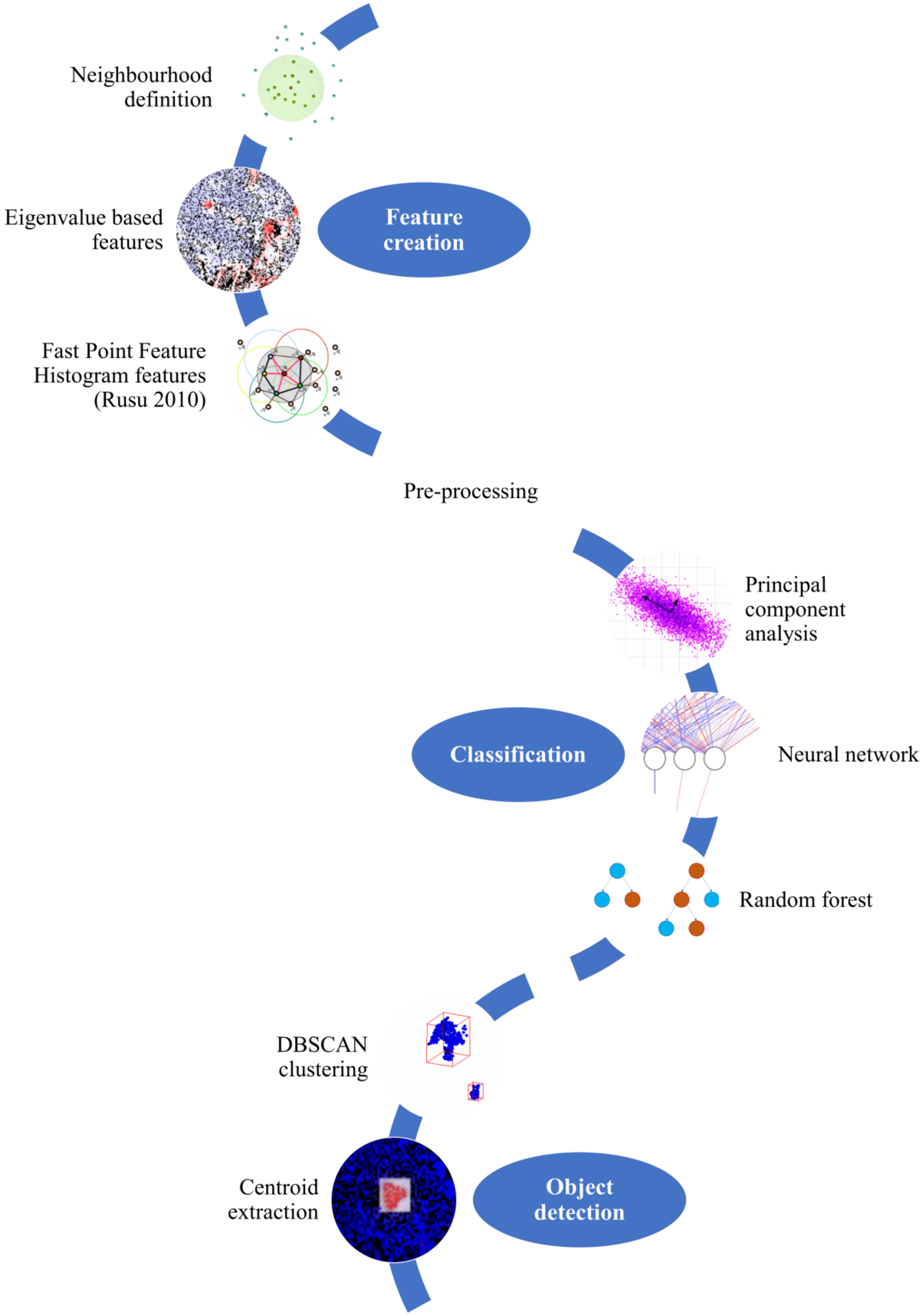

172

173 *Figure 4: Methodology diagram outlining the pipeline used for the task of identification of rock bolts from the laser scan data.*

3.1 Feature creation

Single laser scanned points are not adequate descriptors of the data they represent, as they contain only 3D cartesian coordinates and an intensity value. In isolation, this information is insufficient to describe what type of object this point belongs to; therefore, the point cloud data must be encoded in a way that allows a machine learning algorithm to differentiate between object types. This can be achieved by describing each point in relation to the geometry of its neighbouring points, these descriptors are known as features. The most popular features in the remote sensing community are based on the eigenvalues of the point neighbourhood. Early work by Pauly et al. (2003) and Vandapel et al. (2004) introduced the concept, which was extended by Jutzi and Gross (2009) and Weinmann et al. (2015b). The other common features are proposed by Rusu (2010) and implemented by him in his Point Cloud Library (PCL). This approach computes a fast point feature histogram (FPFH) based on the angular variations between the normals of the points using a Darboux frame (Rusu et al., 2009).

For choosing a point neighbourhood, the dimensions of the object to be detected and the spacing of points in the point cloud determine the optimum value. A typical mechanically anchored rock bolt measures 16cm across the faceplate. Computing the number of neighbours per point over the resampled point cloud using an 8cm radius found the mean number of neighbours to be close to 100, therefore, this is a suitable neighbourhood size to adequately capture the geometry of a rock bolt. Once the neighbourhoods have been defined, descriptive features can be constructed for each point using its neighbours.

Two types of feature sets are calculated for each point in the cloud. The first are the ‘Geometric’ features, described in Weinmann (2016). These include simple 2D and 3D properties of the neighbourhood (density, vertical difference, minimum bounding box), eigenvalue based features which describe the local shape properties of the neighbourhood and 2D accumulation map based features, an overview of each individual feature is given in Table 1. These features were calculated using python code adapted from the MATLAB script published by Weinmann et al. (2015a). The 2D accumulation map features have the highest processing overhead and also are potentially less descriptive for an underground scenario where the hanging wall and foot wall share the same XY coordinates, to investigate, the feature sets were generated both with and without these features. The geometric feature set is powerful as it is understandable and can be easily visualised, Figure 5 shows a small section of hanging wall with the points coloured by the magnitude of different features. It can be seen that certain features are intuitively better at differentiating between 'bolts' and 'not-bolts' for a human interpreter; however, some of the less obvious features may be still be strong descriptors as they can help to separate between false positives and true positives.

The second type of features used are the fast point feature histogram features (FPFH) proposed by Rusu (2010). This type of feature representation uses the relationships between the points in the neighbourhood and their normal vectors to describe the local geometry around the point. This is calculated for each pair of points by defining a fixed Darboux coordinate frame at one point and using it to compute the three angles which define the difference between the normal vectors. The complexity is then reduced by not computing the same neighbourhood pairs for multiple points and instead using a weighting scheme. Finally, the values are binned into a 33 bin histogram. Full derivation of the FPFH is found in Rusu (2009). This step was implemented in C++ with the Point Cloud Library (Rusu and Cousins, 2011).

As the intensity data adds further valuable information about the object, especially underground, two additional features; the intensity of the point itself and the average intensity of the neighbourhood are computed and added to the feature set. As all sets of features are computed individually for each point using the same set K number of neighbours the geometric, FPFH and intensity features can be concatenated, along with the X, Y, Z data for the point and the true class label. The result is a 65-dimensional vector describing the local geometry in a way that can be statistically interpreted by the machine learning classifiers in the next stage, shown in Table 1.

Table 1: Composition of the generated 65 dimensional vector including equations, where k = number of neighbours and λn = eigenvalue n. For classification, the point label column is removed and used as the supervised truth value and the X, Y, Z coordinates do not contribute to the classification. Eigenvalue equations shown are adapted from Weinmann (2016). For brevity, each FPFH value is not shown as they are numbered elements from the same histogram, see Rusu et al. (2009) *for mathematical derivations of these features.*

No	Name	Description	Equation
1	X	X coordinate of point	n/a
2	Y	Y coordinate of point	n/a
3	Z	Z coordinate of point	n/a
4	Label	Point label	n/a
5	Intensity	Reflectance intensity of point	n/a
6	Linearity	How much variance can be explained by only the largest eigenvalue	$(\lambda_1 - \lambda_2)/\lambda_1$
7	Planarity	How much variance can be explained by the two largest eigenvalues	$(\lambda_2 - \lambda_3)/\lambda_1$
8	Scattering	How much neighbourhood variance can be explained by the smallest eigenvalue	λ_3/λ_1
9	Omnivariance	Volumetric point distribution	$\sqrt[3]{(\lambda_1.\lambda_2.\lambda_3)}$
10	Anisotropy	Directional dependence	$(\lambda_1 - \lambda_3)/\lambda_1$
11	Eigenentropy	Order/disorder	$-\lambda_1 \ln(\lambda_1)$ $- \lambda_2 \ln(\lambda_2) - \lambda_3 \ln(\lambda_3)$
12	Sum EVs 3D	Sum of eigenvalues	$\lambda_1 + \lambda_2 + \lambda_3$
13	Curvature change	Local change in curvature	$\lambda_3/(\lambda_1 + \lambda_2 + \lambda_3)$
14	Z values	Absolute height of point	Z
15	KNN radius 3D	Size of the neighbourhood sphere	r_{knn-3D}
16	Density 3D	Points per m^3	$k + 1/(4/3.\pi.r_{knn-3D}^3)$
17	Verticality	The difference from vertical of the Z component of the normal vector	$1 - n_z$
18	Change in Z	Maximum height difference	$Z_{max} - Z_{min}$
19	STD of Z	Standard deviation of heights	$\sigma_{Z,knn-3D}$
20	KNN radius 2D	Size of the neighbourhood circle	r_{knn-2D}
21	Density 2D	Points per m^2	$k + 1/\pi.r_{knn-2D}^2$
22	Sum EVs 2D	Sum of eigenvalues from 2D structural tensor	$\lambda_{1-2D} + \lambda_{2-2D}$
23	EV ratio 2D	Ratio of the 2D eigenvalues	$\lambda_{2-2D}/\lambda_{1-2D}$
24	2D map	Frequency accumulation map	n/a
25	D_Z	Change in Z in accumulation map	n/a
26	Std_Z	Standard deviation of Z in accumulation map	n/a
27	EV_{3d-1}	First 3D eigenvalue	λ_1
28	EV_{3D-2}	Second 3D eigenvalue	λ_2
29	EV_{3D-3}	Third 3D eigenvalue	λ_3
30	EV_{2D-1}	First 2D eigenvalue	λ_{1-2D}
31	EV_{2D-2}	Second 2D eigenvalue	λ_{2-2D}
32	Mean_I	Mean intensity	$\sum \frac{(i_1+i_2 \ldots +i_k)}{k}$
33	$FPFH_1$	FPFH value from bin number 1	n/a
-	- - -	- - -	- - -
65	$FPFH_{33}$	FPFH value from bin number 33	n/a

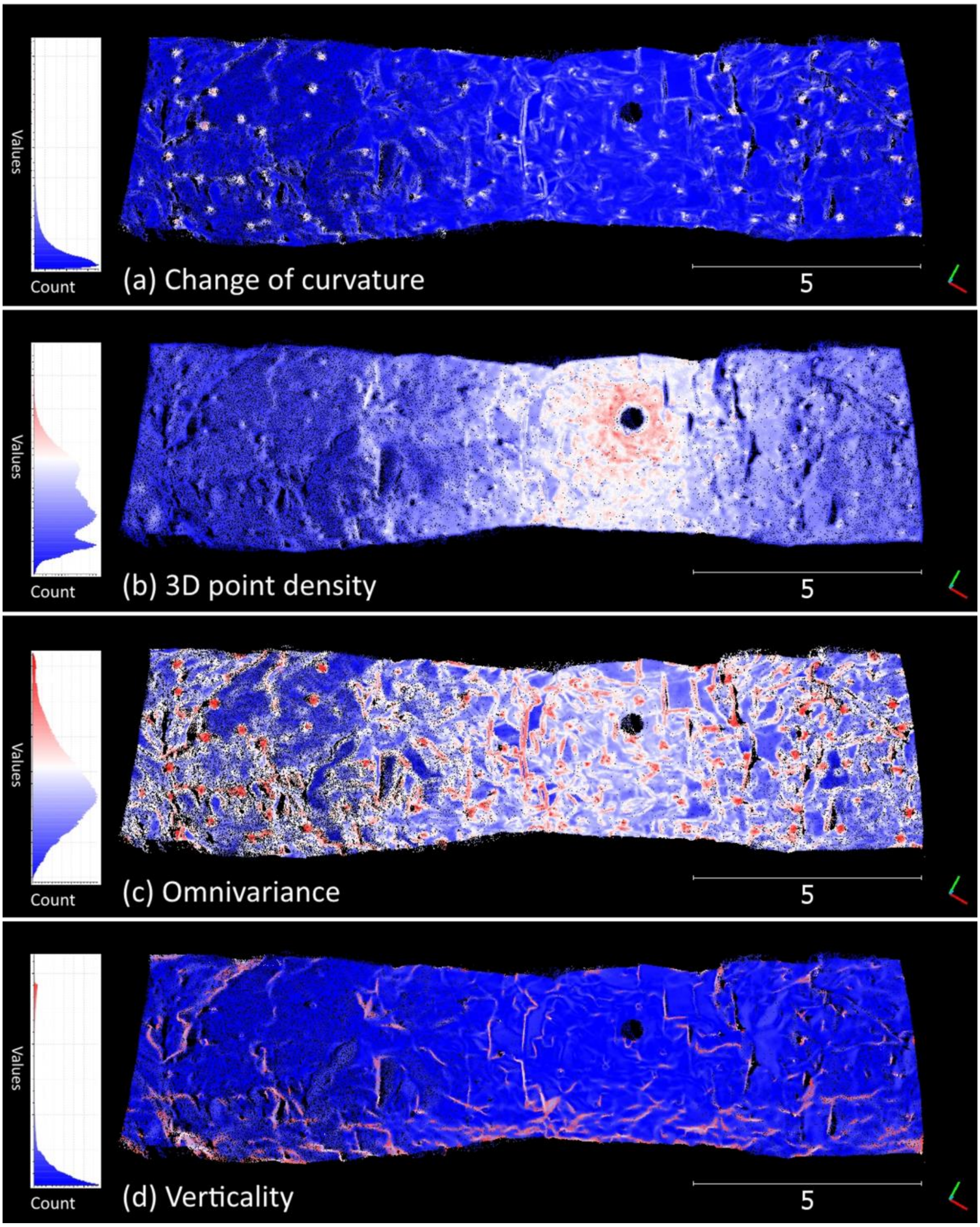

Figure 5: A section of hanging wall showing each point coloured by its feature value. In (a) the areas of high curvature change clearly correspond to rock bolt locations. In (b) the 3D density appears to be more related to the distance from the scanner than the bolt location, indicating that is probably not a particularly effective feature for locating rock bolts. The omnivariance feature shown in (c) is high for the bolts but also high for other areas of discontinuities, especially visible in the vertical lines near the centre of the image, whereas (d) shows the verticality feature which does not spot rock bolts but does have high values in the same areas of non-bolt discontinuities that were highlighted in (c). All scales are relative, and the colour scheme banding runs from blue (lowest) to red (highest) with white as the median value.

3.2 Classification

Once the data has been transformed into meaningful features it can be classified into categories using a variety of machine learning techniques. However, prior to classifier training several pre-processing steps must be carried out to improve the machine interpretability of the data. For the problem of finding rock bolts, the classifier is trained on large hand-labelled where less than 1% of the observed points are rock bolts. If this data were directly used for training, even if the classifier always predicted 'not-bolt' it would achieve 99% accuracy. Of the several possible methods of class rebalancing, the one chosen for this study is down-sampling the majority class. Empirical testing on the cross-validation data found a full downsampling (99% reduction) to match the minority class is not as effective as a less severe 80% reduction of the majority class. After downsampling, each feature is standardised by removing the mean and scaling to unit variance. The final classifier inputs are now a collection of m vectors of dimension n where m corresponds to the number of laser scanned points and n is the number of features in the feature set.

For learning the point representations, Weinmann et al. (2015a) tested many of the most popular types of classifiers including instance based, rule based, probabilistic, max-margin, ensemble and a simple neural network. They found that the ensemble method random forest performed best, which was the method also chosen by Chehata et al. (2009), Niemeyer et al. (2014), Landrieu et al. (2017) and Hackel et al. (2017). For our study, a preliminary test was carried out using multiple machine learning classifiers including Random Forests (RF), Mult-Layer Perceptron (MLP), Support Vector Machines (SVM), Quadratic Discriminant Analysis, Linear Discriminant Analysis and Naive Bayes. The Linear and Quadratic Discriminant Analyses, along with the Naive Bayes proved unable to effectively classify the bolt points and were not considered further. When comparing the remaining three classifiers, the Random Forest produced higher accuracies on the minority bolt class than the Support Vector Machines; these results agree with those found by Bassier et al. (2019), Kogut and Weistock (2019) and Weinmann et al. (2015). However, the MLP outperformed both the SVM and the RF, this is in contrast to the results observed by Bassier et al. (2019) and Weinmann et al. (2015). It is hypothesised that this difference may be due to the larger number of hyperparameters required to produce a stable result from the MLP classifier, as discussed by Nygren and Jasinski (2016). Based on this initial testing, the classifiers chosen for this work were the Random Forest and the MLP. The Random Forest was chosen as it is one of the highest performing classifiers in the literature and has been proven to be capable of achieving robust high accuracy classifications for problems of this type. The MLP was chosen as it showed the best performance in the initial tests and indicated strong generalisation potential when paired with appropriate hyperparameters.

A random forest is a powerful machine learning algorithm based on a randomised forest of decision trees (Breiman, 2001). It has a low number of hyperparameters to tune and is resilient to noise in the data, making it an appropriate choice for remote sensing applications (Pal, 2005). An additional benefit of the random forest classifier is the ability to output a feature importance ranking, allowing for the relative contribution of individual features to the final prediction result to be observed (Strobl et al., 2008). The second classifier, an MLP or artificial neural network, is a node-based architecture which can approximate complex functions by learning weights for every node by a process known as backpropagation (Hecht-Nielsen, 1992). Recent advances in processing power and vast dataset sizes have led to deep learning networks many hundreds of layers deep performing increasingly complex tasks (LeCun et al., 2015).

The structure chosen for the neural network used in this research is informed by the concept of effective capacity. A deep learning algorithm’s effective capacity is its ability to model complexity; good performance is achieved when its effective capacity is appropriate for the complexity of the task and the size of the available training data (Goodfellow et al., 2016). If it has more effective capacity than needed, it will tend to overfit. The task of finding bolt points from multi-dimensional feature vectors requires a relatively small effective capacity, as there are limited generalisation requirements. Combined with the small bespoke training set, an appropriate starting point for the structure was defined as containing no more than three hidden layers with no more than 40 nodes in each layer. Empirical testing was then carried out using a variety of values within this parameter space; stable, effective performance was obtained when the network contained two hidden layers with between 20-30 nodes in the first layer and

5-10 in the second layer. The final chosen structure contained 25 nodes in the first hidden layer and 5 nodes in the second hidden layer.

To decrease processing time, a Principal Component Analysis (PCA) dimensionality reduction (Wold et al., 1987) is performed on the data prior to input, reducing the features from 65 to 40 whilst maintaining 99.4% of the variance. These 40 features are then used as the input to the neural network and are joined to every neuron in the first hidden layer by a weight, with the value of the neuron being the weighted sum of all the features, transformed by the non-linear rectified linear unit (ReLU) function. The second hidden layer has the same structure, with every neuron in each layer connected by weights, and the final output is a binary ('bolt' or 'not-bolt') decision. The network learns by backpropagation using the L-BFGS solver. Both classifications were carried out using the Scikit-learn libraries in Python (Pedregosa et al., 2011).

During model training, suitable values for hyperparameters of the classifiers were determined using a dual strategy. Firstly, a randomised search of the probable value space was carried out, using the Scikit-learn model selection tool 'RandomisedSearchCV' (Pedregosa et al., 2011). Taking the results of this search, empirical testing was then carried out above and below the best random search values to determine the exact hyperparameters choice. This hyperparameter tuning was carried out on the cross-validation section of the dataset via two-fold cross-validation. For the random forest, it was found that only the 'number of estimators' hyperparameter affected the results to any appreciable degree. Therefore, to ease repeatability, the random forest hyperparameters were all kept at the Scikit-learn default values except for the 'number of estimators' hyperparameter which was changed to 200.

The neural network hyperparameters examined included the solver, the activation function and the L2 regularisation term. There was no appreciable difference in accuracy observed from using different solvers, however, the LBFGS converged faster and required fewer additional hyperparameters. Figure 6 shows the results from the empirical testing of the L2 regularisation term and activation function, showing that the best accuracies are obtained with an L2-regularisation term of 1e-4 and the ReLU activation function.

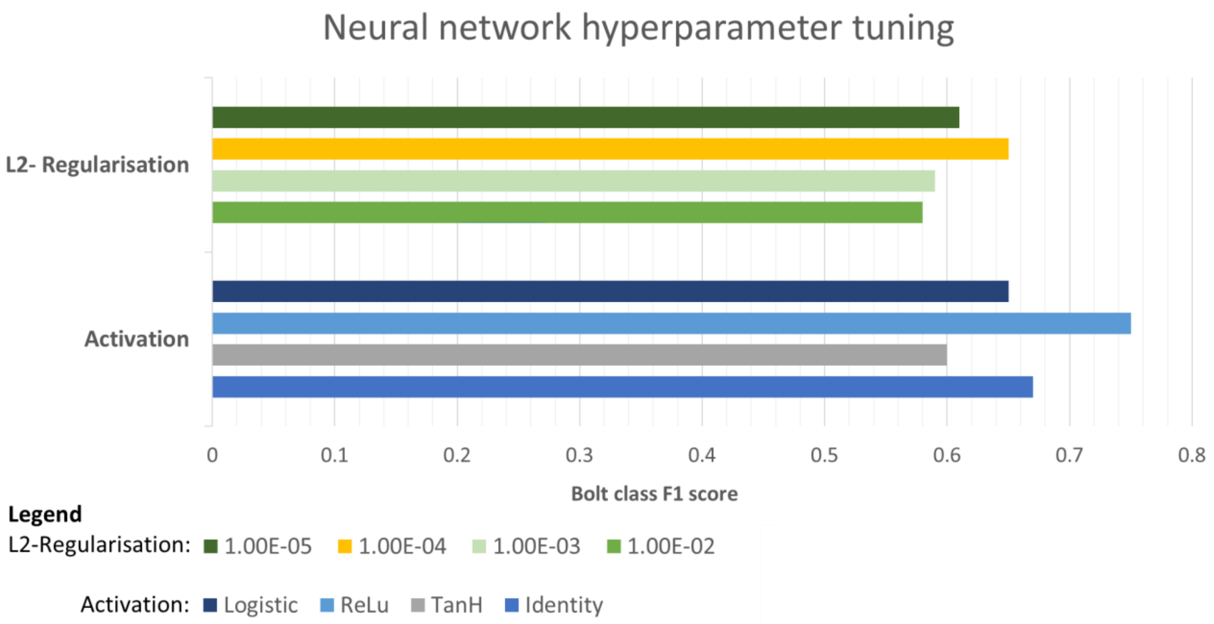

Figure 6: Results from the neural network manual hyperparameter tuning.

Object creation

The type of machine learning used in this research acts on the features derived for each individual point in the cloud. Because there is no spatial connectivity, they suffer from noise due to isolated misclassified points. In the processing pipeline, after the point wise classification, the resulting point cloud is split using the predicted values and the points that have been labelled as 'not-bolt' are now discarded, greatly reducing the dataset size. The remaining cloud now contains all the correctly predicted bolt points and the falsely predicted non-bolt points. From visual examination of this remaining cloud, it can be seen that the point cluster separation is good, with adequate empty space visible between the clusters of predicted points.

Cloud segmentation was carried out using DBSCAN (Density-Based Spatial Clustering of Applications with Noise). This algorithm finds core samples and generates clusters from high density areas adjacent to them, allowing for clusters of any shape (Ester et al., 1996, Schubert et al., 2017). The maximum distance between neighbourhood samples parameter (ε) was set to 5cm and the minimum cluster size was set to 10 points. The ε value was chosen based on the heuristic proposed by Ester et al. (1996) of a suitable value being approximately the distance to the 4^{th} nearest neighbour, in this case 5cm for the 1cm resampled point cloud. The minimum cluster size was set to 10 points; as the ground truth bolt clusters contained between 20-400 points a number set at 50% of the sparsest bolt cluster was a suitable choice of parameter. The Euclidian distance metric was used as the inputs are coordinates in 3D space and the K-D tree algorithm was used to compute the neighbours as the data dimensionality is low.

The final processing step is to calculate the centroid of each cluster to use as the predicted bolt location. The final step is to export these cluster centroids as a X, Y, Z file of only a few kilobytes that can be easily shared with machines and surveyors. This clustering greatly reduces the algorithm's sensitivity to misclassifications in the individual points. Provided at least 10 points from a bolt have been classified correctly the bolt will be detected, reducing missed detections.

4 Results

The performance of the proposed methodology was assessed on both the raw point prediction accuracy and also on the number of bolts correctly detected. The results were evaluated using the measures of precision and recall, along with the F1 score. These metrics were chosen as others such as the overall accuracy are inadequate in cases such as this, where large class imbalances are present in the data. The precision is defined as the measure of what proportion of the positive predictions are correct; it is the number of true positives divided by the number of all predicted positives (true positives and false positives). The recall is a measure of what proportion of actual positives were correctly identified; it is defined as the number of true positives divided by the number of actual positives (true positives and false negatives. The F1 score is the harmonic mean of the precision and recall.

The first experiment tested which set of point feature descriptors provided the most accurate results. It compared the full geometric feature set proposed by Weinmann (2016) consisting of 26 features, a reduced version of this feature set with the accumulation map features removed (23 features), the FPFH features (33 bin histogram), the combined feature sets (59 features) and finally the combined features plus the intensity features (61 features). Table 2 shows the results of the feature set comparison on both classifiers, with the F1 score used as the performance metric. For this test the PCA reduction was not carried out on the neural network dataset to more clearly isolate the effect feature sets have on the results. The random forest classifier also outputted the feature importance rankings, shown in Figure 8 and discussed in Section 5. As the combined features with intensity achieved the highest accuracy, this was the feature set used for the final model which was applied to the unseen test data.

Table 2: F1 scores for differing feature sets. The reduced geometric features refer to the set with the 3 highest computation time features (accumulation maps) removed.

Feature set	**Geometric features full**	**Geometric features reduced**	**FPFH features**	**Combined features**	**Combined features and intensity**
No. features	*26*	*23*	*33*	*59*	*61*
Neural network	0.42	0.41	0.51	0.63	0.64
Random forest	0.49	0.43	0.37	0.56	0.58

Once the feature set choice was finalised, the per point prediction results were examined against the human generated ones for the test data, totalling almost 1.5 million point predictions. These results are given in Table 3. Figure 7 gives a graphical view of the point prediction results. In this figure the footwall has been removed and the viewing angle is directly vertical towards the hanging wall. The predicted bolt points are shown in red, the predicted not-bolt points in blue and the overlaid white squares show the true bolt locations. The left images show the whole point cloud and the right images show just the predicted bolt class points after the removal of the not-bolt predictions. In the right-hand images, anywhere that the red points do not have a corresponding white square overlay indicates incorrect objects classified as bolts, and any white squares without red points indicate missed bolts.

Table 3: Results from the point-wise classifiers in the test dataset.

Neural network	*Predict not-bolt*	*Predict bolt*	**Precision**	0.59
Not-bolt	1471791	6586	**Recall**	0.70
Bolt	4071	9370	**F1 score**	0.64

Random forest	*Predict not-bolt*	*Predict bolt*	**Precision**	0.72
Not-bolt	1475540	2837	**Recall**	0.38
Bolt	6809	6632	**F1 score**	0.58

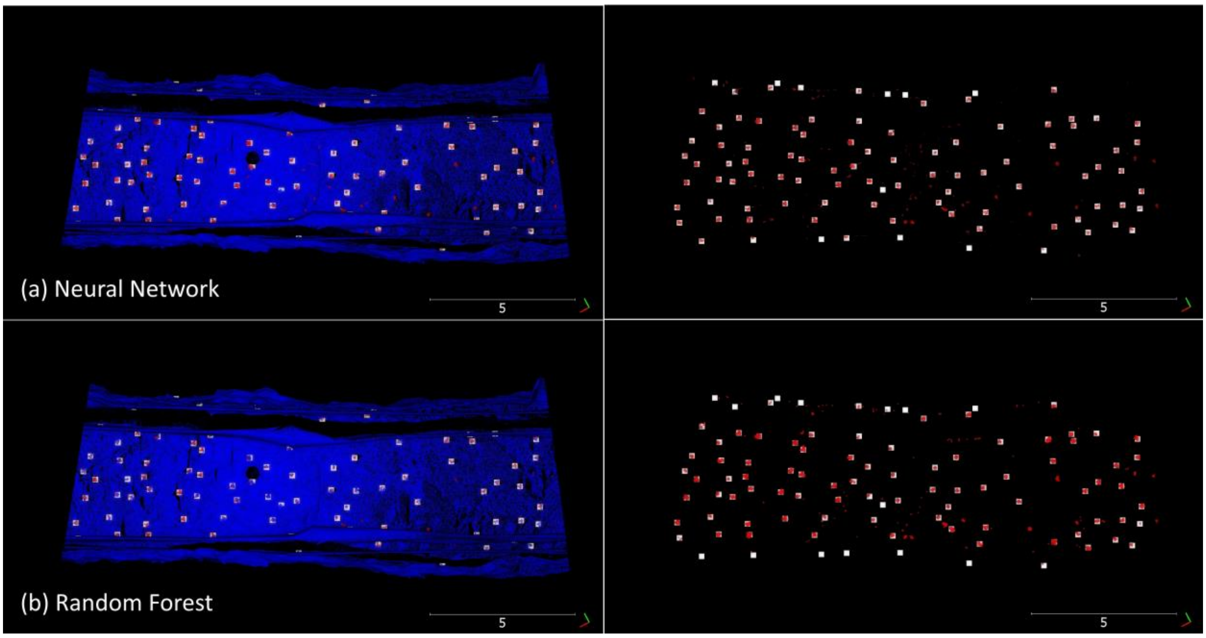

Figure 7: Graphical view of the point cloud classification. The red points are those that the classifier predicts are bolts, the blue points are the classifier predicted as not bolts and the white boxes indicate the actual bolt locations. The left-hand images show the entire classified cloud, whilst the right-hand images show just the points predicted to be bolts.

As can be seen in Table 3, the results, whilst overall positive still contain many misclassified points. To investigate whether the DBSCAN clustering can extract individual bolt object locations to a greater degree of accuracy, the extracted centroids were overlaid with the 101 true bolt centroids and the number of true positives, false positives and false negatives were counted. For this test, the bolt was classed as detected if the human generated and machine generated centroids were within the bolt faceplate radius distance 8cm of each other. These results are given in Table 4.

Table 4: Results of bolt detection algorithm.

Neural network	*Predict Not Bolt*	*Predict Bolt*		
Not Bolt	n/a	**6**	Precision	**0.94**
Bolt	**13**	**88**	Recall	**0.87**
			F1	**0.90**

Random forest	*Predict Not Bolt*	*Predict Bolt*		
Not Bolt	n/a	**3**	Precision	**0.95**
Bolt	**46**	**55**	Recall	**0.54**
			F1	**0.69**

5 Discussion

The feature set test shows that the combined 61 feature set is more effective than either the geometric or FPFH based features applied separately. Using only the geometric feature set, the random forest outperforms the neural network; this agrees with the results obtained by Weinmann et al. (2015a) using the same feature types. Using FPFHs the random forest scores relatively poorly, though the combination does still improve on the score recorded from just the geometric feature set. These results infer that the addition of the FPFH features does contribute to the overall accuracy of the random forest, but that they are less important than the geometric features. To examine the feature contributions further, the feature importances were calculated using the Gini importance method. This technique measures how much the Gini impurity is reduced when using a particular feature, averaged across all trees in the forest (Géron, 2017). The feature importances are then normalised so that the sum of all importances equals one. Figure 8 graphs the feature importances across the classification vector, this shows that the more important features are primarily from the geometric set, though several from the FPFH set also score highly. The highest ranked features (above 0.05) are scattering, absolute height, mean intensity and anisotropy.

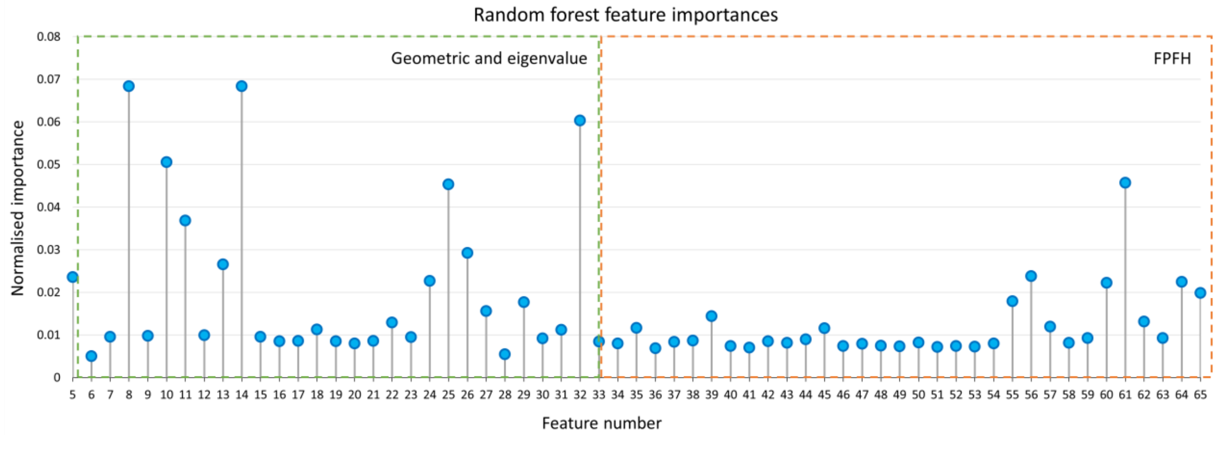

Figure 8: Graph showing the individual feature importances for the random forest classifier. The green box indicates the geometric and eigenvalue based features and the amber box indicates the FPFH features. For details on feature numbers see Table 1.

The neural network classifier cannot output a feature importance ranking; however, from examining the results it appears that the neural network is utilising more of the FPFH set features, as this was the highest non-combined score for all classifier and feature set combinations. The intensity features provided an improvement of 0.02 to both classifiers' scores; these intensity features are some of the simplest to compute and are therefore a strong addition to the feature sets.

The point-wise results are positive despite some misclassifications. This is due to the challenging dataset and the many confusion objects. Most importantly, they contain enough positively identified points to enable the DBSCAN algorithm to detect the actual bolt objects. Primarily the incorrectly identified bolt points (false positives) occurred as isolated points, allowing them to be easily removed by the clustering operation. Only rarely, as in the instance of pipe mounting steelwork which closely resembles a bolt, did the algorithm misclassify enough points in close proximity to create a false positive cluster, as seen in Figure 9, where the cluster inside the red box is large enough to make it through the DBSCAN stage. The isolated incorrect points visible on the hanging wall in Figure 9 will all be removed by the DBSCAN process.

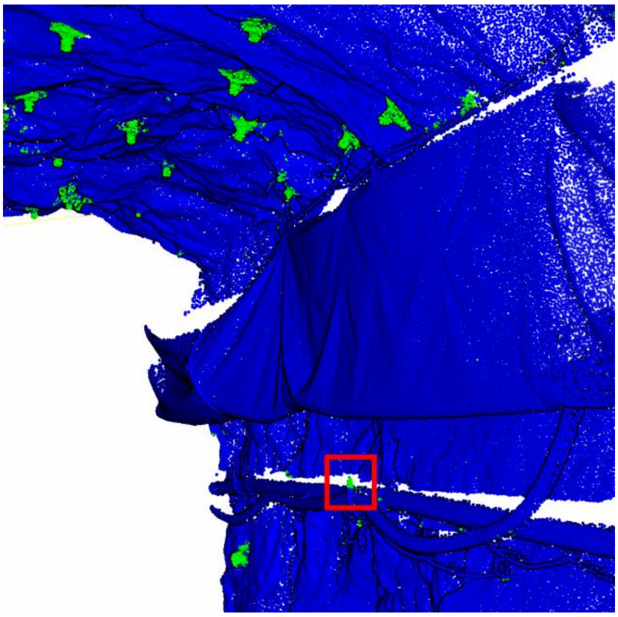

Figure 9: Instance of misclassified cluster of points by the random forest classifier. Blue points are predicted not-bolt, green points are predicted bolt and the red box indicates a piece of pipe mounting bracket incorrectly classified as a bolt.

At the object extraction stage, as both classifiers had only a few false positives, these were manually checked in the original highest resolution scan data to determine if there was in fact a bolt present at that location which had been missed at the labelling stage. From this examination, it appeared that the neural network correctly identified 5 bolts which were badly scanned and highly obscured that had not been picked up at the dataset creation stage. To verify this result, the test area of the tunnel was physically inspected to determine the ground truth. All bolts visible from the scanner positions were verified, confirming the 96 human detected bolts and the 5 bolts missed by the human labelling exercise. Bolts entirely hidden from the scanner position were not included as these were not detectable from the scan data by a human or an algorithm.

This brought the number of true bolts in the test data up to 101. This demonstrates the value of machine learning technologies for automated quality assurance and quality control as in these difficult cases the neural network surpassed the human inspector. The testing dataset was then used to estimate the level of label noise present in the training dataset. The test dataset label noise was ~5% at the cluster/object level (5 missed out of 101 total) and ~3% at the individual point level (471 missed out of 13,912 total). The figures are expected to be far lower for the training dataset as the mislabelled points are all in the 'not bolt' class, which has been randomly resampled to contain only 20% of its points. Neural networks and random forests have been shown to be highly robust to label noise below 10% (Folleco et al. 2009, Pelletier et al. 2017), therefore, the small number of mislabelled points in the training dataset is not expected to have has a meaningful impact on the classifier training. Comparing the human result to the neural network, the human is still superior with a precision of 1 and a recall of 0.95; however, in a real world inspection case, the human takes much longer to identify the bolts, suffers from fatigue and still cannot detect every bolt. Figure 10 (a) and (b) show an example a bolt missed by the human operator but found by the neural network and Figure 10 (c) shows an actual incorrect detection by the neural network.

The false negatives from the neural network also were examined, and it was found that 10 out of the 11 missed detections were low bolts on the sidewall. From this, we can infer that that the Z values and the relatively few sidewall bolts compared to roof bolts in the training data are influencing the model's decision making. Future work will investigate whether this result can be improved by adding more sidewall training data examples through augmentation or by removing the features related to absolute Z value. Future work would also consider reimplementing the pipeline in C++ using the PCL libraries for increased speed for a production mining environment.

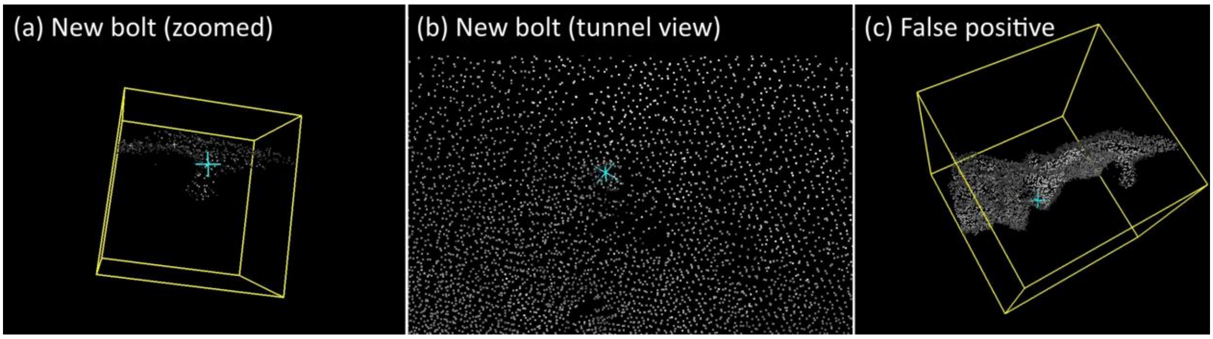

Figure 10: Examintation of false negatives and false positives. (a) shows the flase negative bolt zoomed and extracted to a specific angle and (b) shows how the false negative appearsto a human in the full tunnel dataset. (c) shows a sharp discontinuity (false poitive) that has been mistaken for a bolt by the classifier.

6 Conclusion

This paper describes a methodology to automatically detect supporting rock bolts from laser scan data. After the scans have been extracted from the instrument, the workflow is implemented entirely with open source software. Our methodology is customised to the underground environment and improves upon previously published surface applications by utilising a larger feature set and robust clustering to address the challenges from noise, confusion objects and multiple Z values present in a typical excavated tunnel. The neural network classifier produced the strongest point-wise classification results, allowing the DBSCAN algorithm to successfully locate the candidate bolt objects. Further work will focus on extending this approach to other mining datasets gathered with different types of 3D laser scanners including low cost mobile solutions. The bolt location output files could be used for multiple applications including verifying bolting patterns that have been installed to specification, recording spot bolting locations for geotechnical reference and for linking the onboard hole information recorded by bolting machines to a real world coordinate. These applications offer mining companies valuable opportunities to embrace new technologies for improved productivity and safety in a digitally connected world.

Funding: This research was carried out as part of a PhD studentship funded by the University of Exeter.

J. Gallwey: Methodology, Writing-Original draft preparation, Investigation, Software **M. Eyre**: Conceptualization, Writing- Reviewing and Editing, Supervision. **J. Coggan**: Supervision, Project Administration, Writing- Reviewing and Editing.

References

Agrawal, A., Nakazawa, A., Takemura, H., 2009. MMM-classification of 3D Range Data, in: IEEE International Conference on Robotics and Automation. Kobe, pp. 2003–2008

Anguelov, D., Taskarf, B., Chatalbashev, V., Koller, D., Gupta, D., Heitz, G., Ng, A., 2005. Discriminative learning of Markov random fields for segmentation of 3D scan data. Comput. Vis. Pattern Recognition, 2005. CVPR 2005. IEEE Comput. Soc. Conf. 2, 169–176 vol. 2. https://doi.org/10.1109/CVPR.2005.133

Attard, L., Debono, C.J., Valentino, G., Di Castro, M., 2018. Tunnel inspection using photogrammetric techniques and image processing: A review. ISPRS J. Photogramm. Remote Sens. 144, 180–188. https://doi.org/10.1016/J.ISPRSJPRS.2018.07.010

Balado, J., Díaz-Vilariño, L., Arias, P., González-Jorge, H., 2018. Automatic classification of urban ground elements from mobile laser scanning data. Autom. Constr. 86, 226–239. https://doi.org/https://doi.org/10.1016/j.autcon.2017.09.004

Bassier, M., Van Genechten, B., Vergauwen, M., 2019. Classification of sensor independent point cloud data of building objects using random forests. J. Build. Eng. 21, 468–477. https://doi.org/10.1016/j.jobe.2018.04.027

Behley, J., Kersting, K., Schulz, D., Steinhage, V., Cremers, A.B., 2010. Learning to hash logistic regression for fast 3D scan point classification. IEEE/RSJ 2010 Int. Conf. Intell. Robot. Syst. IROS 2010 - Conf. Proc. 5960–5965. https://doi.org/10.1109/IROS.2010.5650093

Blomley, R., Jutzi, B., Weinmann, M., 2016. Classification of Airborne Laser Scanning Data Using Geometric Multi-Scale Features and Different Neighbourhood Types. ISPRS Ann. Photogramm. Remote Sens. Spat. Inf. Sci. III–3, 169–176. https://doi.org/10.5194/isprsannals-III-3-169-2016

Body, D., 2014. The Changing Face of Surveying within the Mining Industry [WWW Document]. URL https://www.bentley.com/-/media/A633A2E0F9EB48D190DE94E3F1529CFF.ashx (accessed 10.03.20)

Breiman, L., 2001. Random Forests. Mach. Learn. 45, 5–32. https://doi.org/10.1023/A:1010933404324

Chehata, N., Guo, L., Mallet, C., 2009. Airborne LIDAR feature selection for urban classification using random forests. Int. Arch. Photogramm. Remote Sens. Spat. Inf. Sci. 38.

Chen, S., Walske, M.L., Davies, I.J., 2018. Rapid mapping and analysing rock mass discontinuities with 3D terrestrial laser scanning in the underground excavation. Int. J. Rock Mech. Min. Sci. 110, 28–35. https://doi.org/https://doi.org/10.1016/j.ijrmms.2018.07.012

Ester, M., Kriegel, H.-P., Sander, J., Xu, X., 1996. A Density-Based Algorithm for Discovering Clusters a Density-Based Algorithm for Discovering Clusters in Large Spatial Databases with Noise, in: Proceedings of the Second International Conference on Knowledge Discovery and Data Mining, KDD'96. AAAI Press, pp. 226–231

Eyre, M., Wetherelt, A., Coggan, J., 2016. Evaluation of automated underground mapping solutions for mining and civil engineering applications. J. Appl. Remote Sens. 10, 1–18. https://doi.org/10.1117/1.JRS.10.046011

Folleco, A.A., Khoshgoftaar, T.M., Van Hulse, J., Napolitano, A., 2009. Identifying learners robust to low quality data. Inform. 33, 245–259.

Ganić, A., Milutinović, A., Tokalić, R., Ognjanović, S., 2011. Measuring methods for cross sections of underground mine chambers. Podzemn. Rad. 0

Géron, A., 2017. Hands-On Machine Learning with Scikit-Learn & Tensorflow, 1st ed. O'Reilly, Sebastopol.

Gikas, V., 2012. Three-dimensional laser scanning for geometry documentation and construction management of highway tunnels during excavation. Sensors (Switzerland) 12, 11249–11270. https://doi.org/10.3390/s120811249

Girardeau-Montaut, D., 2016. Cloud compare documentation [WWW Document]. URL http://www.cloudcompare.org/doc/wiki/index.php?title=Main_Page (accessed 11.02.20)

Goodfellow, I., Bengio, Y., Courville, A., 2016. Deep Learning. MIT Press, Cambridge MA.

Hackel, T., Wegner, J.D., Schindler, K., 2017. Joint classification and contour extraction of large 3D point clouds. ISPRS J. Photogramm. Remote Sens. 130, 231–245. https://doi.org/10.1016/j.isprsjprs.2017.05.012

Hecht-Nielsen, R., 1992. III.3 - Theory of the Backpropagation Neural Network**Based on “nonindent” by Robert Hecht-Nielsen, which appeared in Proceedings of the International Joint Conference on Neural Networks 1, 593–611, June 1989. © 1989 IEEE., in: Wechsler, H. (Ed.), Neural Networks for Perception. Academic Press, pp. 65–93. https://doi.org/https://doi.org/10.1016/B978-0-12-741252-8.50010-8

Hoek, E., Brown, E., 1980. Underground Excavations in Rock. Institution of Mining and Metallurgy, London ISBN 0900488549

Huang, H., Li, Q., Zhang, D., 2018. Deep learning based image recognition for crack and leakage defects of metro shield tunnel. Tunn. Undergr. Sp. Technol. 77, 166–176. https://doi.org/10.1016/j.tust.2018.04.002

Jutzi, B., Gross, H., 2009. Nearest neighbour classification on laser point clouds to gain object structures from buildings. ISPRS Hann. Work. 2009 High-Resolution Earth Imaging Geospatial Inf. XXXVIII, 6

Kogut, T., Weistock, M., 2019. Classifying airborne bathymetry data using the Random Forest algorithm. Remote Sens. Lett. 10, 874–882. https://doi.org/10.1080/2150704X.2019.1629710

Landrieu, L., Raguet, H., Vallet, B., Mallet, C., Weinmann, M., 2017. A structured regularization framework for spatially smoothing semantic labelings of 3D point clouds. ISPRS J. Photogramm. Remote Sens. 132, 102–118. https://doi.org/10.1016/j.isprsjprs.2017.08.010

LeCun, Y., Bengio, Y., Hinton, G., 2015. Deep learning. Nature 521, 436–444.

https://doi.org/10.1038/nature14539

Lehtomäki, M., Jaakkola, A., Hyyppä, J., Kukko, A., Kaartinen, H., 2010. Detection of vertical pole-like objects in a road environment using vehicle-based laser scanning data. Remote Sens. 2, 641–664. https://doi.org/10.3390/rs2030641

Lehtomäki, M., Jaakkola, A., Hyyppä, J., Lampinen, J., Kaartinen, H., Kukko, A., Puttonen, E., Hyyppä, H., 2016. Object Classification and Recognition From Mobile Laser Scanning Point Clouds in a Road Environment. IEEE Trans. Geosci. Remote Sens. 54, 1226–1239. https://doi.org/10.1109/TGRS.2015.2476502

Li, C.C., 2017. Principles of rockbolting design. J. Rock Mech. Geotech. Eng. 9, 396–414. https://doi.org/10.1016/j.jrmge.2017.04.002

Long, N.Q., Buczek, M.M., Hien, L.P., Szlapińska, S.A., Nam, B.X., Nghia, N.V., Cuong, C.X., 2018. Accuracy assessment of mine walls' surface models derived from terrestrial laser scanning. Int. J. Coal Sci. Technol. 5, 328–338. https://doi.org/10.1007/s40789-018-0218-1

Martínez-Sánchez, J., Puente, I., González-Jorge, H., Riveiro, B., Arias, P., 2016. Automatic thickness and volume estimation of sprayed concrete on anchored retaining walls from terrestrial LIDAR data. Int. Arch. Photogramm. Remote Sens. Spat. Inf. Sci. - ISPRS Arch. 41, 521–526. https://doi.org/10.5194/isprsarchives-XLI-B5-521-2016

Maturana, D., Scherer, S., 2015. VoxNet: A 3D convolutional neural network for real-time object recognition. IEEE/RSJ Int. Conf. Intell. Robot. Syst. 922–928. https://doi.org/10.1109/IROS.2015.7353481

Niemeyer, J., Rottensteiner, F., Soergel, U., 2014. Contextual classification of lidar data and building object detection in urban areas. ISPRS J. Photogramm. Remote Sens. 87, 152–165. https://doi.org/10.1016/j.isprsjprs.2013.11.001

Nygren, P., Jasinski, M., 2016. A Comparative Study of Segmentation and Classification Methods for 3D Point Clouds. University of Gothenburg.

Öberg, F., 2013. Method and system for monitoring and documenting installation of rock reinforcement bolt. US 8,606,542 B2

Pal, M., 2005. Random forest classifier for remote sensing classification. Int. J. Remote Sens. 26, 217–222. https://doi.org/10.1080/01431160412331269698

Pauly, M., Keiser, R., Gross, M., 2003. Multi-scale Feature Extraction on Point-Sampled Surfaces. Comput. Graph. Forum 22, 281–289. https://doi.org/10.1111/1467-8659.00675

Pedregosa, F., Varoquaux, G., Gramfort, A., Michel, V., Thirion, B., Grisel, O., Blondel, M., Prettenhofer, P., Weiss, R., Dubourg, V., Vanderplas, J., Passos, A., Cournapeau, D., Brucher, M., Perrot, M., Duchesnay, E., 2011. Scikit-learn: Machine Learning in Python. J. Mach. Learn. Res. 12, 2825–2830

Pelletier, C., Valero, S., Inglada, J., Champion, N., Sicre, C.M., Dedieu, G., 2017. Effect of training class label noise on classification performances for land cover mapping with satellite image time series. Remote Sens. 9. https://doi.org/10.3390/rs9020173

Qi, C.R., Su, H., Mo, K., Guibas, L.J., 2016. PointNet: Deep Learning on Point Sets for 3D Classification and Segmentation, in: 4th International Conference on 3D Vision, 3DV 2016. pp. 601–610. https://doi.org/10.1109/3DV.2016.68

Rau, J.Y., Jhan, J.P., Hsu, Y.C., 2015. Analysis of oblique aerial images for land cover and point cloud classification in an Urban environment. IEEE Trans. Geosci. Remote Sens. 53, 1304–1319. https://doi.org/10.1109/TGRS.2014.2337658

Riegler, G., Ulusoy, A.O., Geiger, A., 2017. OctNet: Learning deep 3D representations at high resolutions. Proc. - 30th IEEE Conf. Comput. Vis. Pattern Recognition, CVPR 2017 2017-Janua, 6620–6629. https://doi.org/10.1109/CVPR.2017.701

Rusu, R.B., 2010. Semantic 3D Object Maps for Everyday Manipulation in Human Living Environments. Künstliche Intelligenz 24, 345–348. https://doi.org/10.1007/s13218-010-0059-6

Rusu, R.B., Blodow, N., Beetz, M., 2009. Fast Point Feature Histograms (FPFH) for 3D registration.

2009 IEEE Int. Conf. Robot. Autom. 3212–3217. https://doi.org/10.1109/ROBOT.2009.5152473

Rusu, R.B., Cousins, S., 2011. 3D is here: Point Cloud Library (PCL), in: 2011 IEEE International Conference on Robotics and Automation. pp. 1–4. https://doi.org/10.1109/ICRA.2011.5980567

Schach, R., Garshol, K., Heltzen, A.M., 1979. Rock Bolting: A Practical Handbook, Pergamon Press, Oxford, ISBN 0080225039

Schubert, E., Sander, J., Ester, M., Kriegel, H.P., Xu, X., 2017. DBSCAN Revisited, Revisited: Why and How You Should (Still) Use DBSCAN. ACM Trans. Database Syst. 42. https://doi.org/10.1145/3068335

Soilán, M., Riveiro, B., Martínez-Sánchez, J., Arias, P., 2017. Segmentation and classification of road markings using MLS data. ISPRS J. Photogramm. Remote Sens. 123, 94–103. https://doi.org/10.1016/j.isprsjprs.2016.11.011

Soilán, M., Sánchez-Rodríguez, A., Del Río-Barral, P., Perez-Collazo, C., Arias, P., Riveiro, B., 2019. Review of laser scanning technologies and their applications for road and railway infrastructure monitoring. Infrastructures 4. https://doi.org/10.3390/infrastructures4040058

Strobl, C., Boulesteix, A.-L., Kneib, T., Augustin, T., Zeileis, A., 2008. Conditional variable importance for random forests. BMC Bioinformatics 9, 307. https://doi.org/10.1186/1471-2105-9-307

Tan, K., Cheng, X., Ju, Q., Wu, S., 2016. Correction of Mobile TLS Intensity Data for Water Leakage Spots Detection in Metro Tunnels. IEEE Geosci. Remote Sens. Lett. 13, 1711–1715. https://doi.org/10.1109/LGRS.2016.2605158

Triebel, R., Kersting, K., Burgard, W., 2006. Robust 3D scan point classification using associative Markov networks. Proc. - IEEE Int. Conf. Robot. Autom. 2006, 2603–2608. https://doi.org/10.1109/ROBOT.2006.1642094

van der Merwe, J.W., Andersen, D.C., 2013. Applications and benefits of 3D laser scanning for the mining industry . J. South. African Inst. Min. Metall.

Vandapel, N., Huber, D., Kapuria, A., Hebert, M., 2004. Natural terrain classification using 3-d ladar data. IEEE Int. Conf. Robot. Autom. 2004. Proceedings. ICRA ’04. 2004 5117–5122. https://doi.org/10.1109/ROBOT.2004.1302529

Weinmann, M., Jutzi, B., Hinz, S., Mallet, C., 2015a. Semantic point cloud interpretation based on optimal neighborhoods, relevant features and efficient classifiers. ISPRS J. Photogramm. Remote Sens. 105, 286–304. https://doi.org/10.1016/j.isprsjprs.2015.01.016

Weinmann, M., Urban, S., Hinz, S., Jutzi, B., Mallet, C., 2015b. Distinctive 2D and 3D features for automated large-scale scene analysis in urban areas. Comput. Graph. 49, 47–57. https://doi.org/10.1016/j.cag.2015.01.006

Weinmann, M., 2016. Reconstruction and analysis of 3D scenes: From irregularly distributed 3D points to object classes. Reconstr. Anal. 3D Scenes From Irregularly Distrib. 3D Points to Object Classes 1–233. https://doi.org/10.1007/978-3-319-29246-5

Weinmann, Martin, Weinmann, Michael, Mallet, C., Brédif, M., 2017. A classification-segmentation framework for the detection of individual trees in dense MMS point cloud data acquired in urban areas. Remote Sens. 9. https://doi.org/10.3390/rs903277

Wold, S., Esbensen, K., Geladi, P., 1987. Principal component analysis. Chemom. Intell. Lab. Syst. 2, 37–52. https://doi.org/https://doi.org/10.1016/0169-7439(87)80084-9

Xu, T., Xu, L., Li, X., Yao, J., 2018. Detection of Water Leakage in Underground Tunnels Using Corrected Intensity Data and 3D Point Cloud of Terrestrial Laser Scanning. IEEE Access 6, 32471–32480. https://doi.org/10.1109/ACCESS.2018.2842797

Yang, B., Fang, L., Li, J., 2013. Semi-automated extraction and delineation of 3D roads of street scene from mobile laser scanning point clouds. ISPRS J. Photogramm. Remote Sens. 79, 80–93. https://doi.org/10.1016/j.isprsjprs.2013.01.016

Zhao, S., Zhang, D.M., Huang, H.W., 2020. Deep learning–based image instance segmentation for moisture marks of shield tunnel lining. Tunn. Undergr. Sp. Technol. https://doi.org/10.1016/j.tust.2019.103156